Synthesis and characterization of three co-crystals of bis(benzimidazole) derivatives with aromatic dicarboxylic acids

Shang-Zhuo Wu[1] · Qiang Yu[1] · Yue-Hua Li[1] · Guang-Hua Cui[1] (ORCID)

Abstract

Combination of three aromatic carboxylic acids (5-nitroisophthalic acid (H_2nip), 2,6-naphthalenedicarboxylic acid (H_2ndc), tetrabromoterephthalic acid (H_2tbta)) and flexible bis(benzimidazole) derivatives (1,6-bis(2-methylbenzimidazol-1-yl) hexane (L1), 1,2-bis(2-methylbenzimidazol-1-ylmethyl)benzene (L2), 1,4-bis(2-methylbenzimidazol-1-yl)butane (L3)), three co-crystals [(H_2L1)$^{2+}$·2(Hnip)$^-$·H_2O] (**1**), [(L2)·(H_2ndc)] (**2**) and [(H_2L3)$^{2+}$·(tbta)$^{2-}$] (**3**) were synthesized hydrothermally. Single-crystal X-ray diffraction, elemental analysis and IR spectra are employed to characterize **1**, **2** and **3**. The 2D fingerprint plots and Hirshfeld surfaces of **1**, **2** and **3** indicate that the 3D supramolecular network for **1** was generated by N–H···O, O–H···O, C–H··O hydrogen bonds and $\pi-\pi$ interactions, the 2D sheet for **2** was produced by O–H···N hydrogen bonds and $\pi-\pi$ interactions, and C–H···O hydrogen bonds make structures more stable. For **3**, the 2D supramolecular layer was yielded by N–H···O, C–H···O hydrogen bond interactions. Furthermore, thermogravimetric analyses and photoluminescence properties of three compounds were presented.

Keywords Bis(benzimidazole) · Crystal structures · Hirshfeld surfaces · Photoluminescent properties · Supramolecular interaction

✉ Guang-Hua Cui
 tscghua@126.com

1   Hebei Key Laboratory for Environment Photocatalytic and Electrocatalytic Materials, College of Chemical Engineering, North China University of Science and Technology, No. 21 Bohai Road, Caofeidian new-city, Tangshan 063210, Hebei, People's Republic of China

Introduction

In the area of crystal engineering, the design and synthesis of supramolecular compounds get great attraction, which demonstrated inspiring potential applications in pharmaceutical, luminescence materials, solid-state organic synthesis, molecular electronics and electrical conductivity [1–4]. Under such circumstances, some supramolecular compounds adopting non-covalent intermolecular interactions were successfully constructed through self-assembly [5–7]. In the non-covalent intermolecular interactions, the most reliable and useful interaction has demonstrated to be the hydrogen bonding, due to its directionality and strength [8–10]. As multi-component crystals, because of the different capabilities of hydrogen bonding, the properties and structures of supramolecular complexes may be significantly affected by the combination of various organic components with distinct orientations and functional groups [11, 12]. Sang Loon Tan and Edward R.T. Tiekink use N, N'-bis(pyridin-4-ylmethyl)oxamide and glacial acetic acid to synthesize a co-crystal, in which the hydrogen bond has a major influence on the structure of the co-crystal [13]. In addition, Sun group reported three co-crystals which were synthesized by the reaction of pyrazinamide with *m*-hydroxybenzoic acid, *p*-hydroxybenzoic acid and 3,4-dihydroxybenzoic acid [14]. In those co-crystals, the structures were stabilized by the strong O–H···O, N–H···O hydrogen bonding interactions. Nevertheless, researches on the supramolecular architectures of bis(benzimidazole) derivatives are still insufficient [15–18]. In the series of bis(2-methylbenzimidazole) compounds, the methyl substituent is capable of effectively enhance the electron donating ability [19]. In addition, the large conjugated π−system and imidazole ring can engage π−π stacking interactions and hydrogen bonding. Furthermore, in terms of our understanding, the −COOH groups moieties represent the excellent and widely researched functional group, which can compose directional and robust hydrogen bonds; aromatic carboxylic acids, such as 5-nitroisophthalic acid (H_2nip), 2,6-naphthalenedicarboxylic acid (H_2ndc), tetrabromoterephthalic acid (H_2tbta) (Scheme 1), are usually served as organic components in the crystal engineering [20–22].

In supramolecular networks, the Hirshfeld surfaces analysis is a useful approach to reveal the intermolecular interactions [23–25]. This way provides a concise
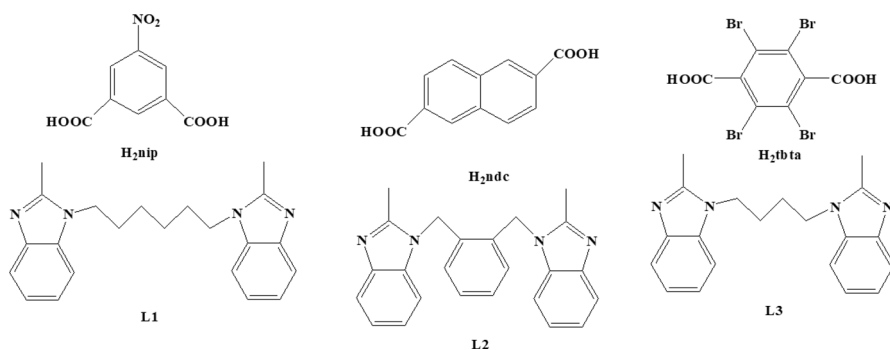
Scheme 1 The structures of the molecular components of compounds **1–3**

method to acquire all the intermolecular interaction on crystal packing. The information provided by the breakdown of corresponding 2D fingerprint plot not only contains the sort of intermolecular interactions in crystal structures, also feedback this message through a convenient color chart.

Here, three supramolecular compounds have been synthesized and characterized for the purpose of exploring their properties, structures and intermolecular interactions, namely $[(H_2L1)^{2+}\cdot2(Hnip)^-\cdot H_2O]$ (**1**), $[(L2)\cdot(H_2ndc)]$ (**2**), $[(H_2L3)^{2+}\cdot(tbta)^{2-}]$ (**3**) (1,6-bis(2-methylbenzimidazol-1-yl)hexane (L1), 1,2-bis(2-methylbenzimidazol-1-ylmethyl)benzene (L2), 1,4-bis(2-methylbenzimidazol-1yl)butane (L3)) (Scheme 1). The non-covalent information such as hydrogen bonding and $\pi-\pi$ interactions is investigated using Hirshfeld surface-based tool. In addition, thermogravimetric analysis (TGA) and fluorescence spectra of three compounds are performed.

Experimental

Materials and measurements

All the chemicals employed here were acquired from commercial method and directly applied without further purification. The PerkinElmer 240C analyzer was taken to determine the contents of C, N and H. At the range 4000–400 cm^{-1}, FTIR spectra were measured in an Avatar 360 (Nicolet) spectrophotometer with KBr pellets. The photoluminescence spectra in solid state were surveyed on an Edinburgh instruments FS5 spectrophotometer. Under an N_2 atmosphere, the NETZSCH STA 449 F3 differential thermal analyzer was employed to perform the TGA at a rate of 10 °C/min from room temperature to 800 °C.

Preparation of the compounds

$[(H_2L1)^{2+}\cdot2(Hnip)^-\cdot H_2O]$ (1)

A mixture of L1 (0.1 mmol), H_2nip (0.2 mmol) and H_2O (10 mL) was put in a 25-mL Teflon-lined stainless steel vessel. Seal the mixture and heat at 140 °C for 3 days, then the mixture was cooled to room temperature at 5 °C/h. Colorless block crystals of **1** were gathered with the yield 42% (based on L1). Anal. Calcd. For $C_{38}H_{38}N_6O_{13}$ (Mr = 786.74): C 57.96%, H 4.83%, N 10.68%. Found: C 57.82, H 5.04, N 10.46%. IR (KBr, cm^{-1}): 3448(s), 3092(w), 1704(w), 1630(s), 1531(m), 1460(m), 1376(s), 1197(w), 761(m).

$[(L2)\cdot(H_2ndc)]$ (2)

The synthesis process of **2** is similar to the synthetic of **1**, in addition to using L2 (36.6 mg, 0.1 mmol) and H_2ndc (43.2 mg, 0.2 mmol) instead of L1 and H_2nip, respectively. Colorless block crystals of **2** were received with yield 40% (based on L2). Anal. Calcd. For $C_{36}H_{30}N_4O_4$ (Mr = 582.64): C 74.21, H 5.19, N 9.62%. Found:

C 74.39, H 5.34, N 9.73%. IR (KBr, cm^{-1}): 3425(m), 3000(s), 1690(s), 1600(m), 1508(w), 1424(m), 1293(s), 1191(s), 748(s).

[(H$_2$L3)$^{2+}$·(tbta)$^{2-}$] (3)

The synthesis process of **3** is similar to **1**, apart from that L1 and H$_2$nip are substituted by L3 and H$_2$tbta, respectively. Colorless block crystals of **3** were obtained with yield 44% (based on L3). Anal. Calcd for C$_{28}$H$_{24}$Br$_4$N$_4$O$_4$ (Mr = 800.15): C 42.01, H 2.99, N 7.00%. Found: C 42.21, H 2.73, N 6.82%. IR (KBr, cm^{-1}):3452(s), 3100(m), 1640(s), 1465(m), 1423(m), 1301(m), 1075(m), 855(s), 754(m).

X-ray Crystal Structure Determination

The Bruker Smar1000 CCD area-detector diffractometer taking graphite-monochromated Mo-Kα radiation ($\lambda = 0.71073$ Å) with ω scan mode is used to collect the single-crystal X-ray diffraction data of complexes **1**, **2** and **3** at 293 K. The direct methods are adopted to solve the structures of **1**, **2** and **3**, the refinements use full-matrix least-squares techniques of SHELX package based on F^2 [26]. All non-hydrogen atoms are treated anisotropically. The H atoms of water molecules were added by difference Fourier maps and with fixed displacement parameters. The other H atoms were geometrically generated using a riding model and isotropically refined. Their main crystallographic details of **1**, **2** and **3** are listed in Table 1. The selected bond lengths and angles of the three complexes are summarized in Table S1. The summary of geometrical parameters for hydrogen bonds and $\pi-\pi$ interactions is given in Tables 2 and 3.

Hirshfeld surface calculations

The CrystalExplorer program is exploited to compute the molecular Hirshfeld surfaces [27, 28]. All Hirshfeld surfaces (d_{norm}, *Shape index* and *Curvedness*) are generated in a standard (high) surface resolution. Input the CIF files of **1**, **2** and **3** into the CrystalExplorer program, and all the bond lengths with hydrogen are automatically revised to the typical standard neutron value (O–H = 0.983 Å, N–H = 1.009 Å and C–H = 1.083 Å). Each crystal has its own Hirshfeld surface due to the spherical atomic electron densities and the given structure. The intermolecular interactions are compared using a red–blue–white color scheme in the 3D d_{norm} surface: red areas express shorter contacts than van der Waals (vdW) distances and the negative d_{norm} value, blue regions denote longer contacts than van der Waals (vdW) separations with a positive d_{norm} value and white areas are the separation of contacts exactly corresponding to the vdW separations with the d_{norm} value of zero. The *Shape index* is the most sensitive to very subtle changes in surface shape, the red triangles on them (above the plane of the molecule) demonstrate atoms of the $\pi\cdots$stacked molecule above them, and the blue triangles reveal the ring atoms of these molecules inside these surfaces. In the *Curvedness*, the low curvature is indicated by the flat area of the surface, high values of curvedness are represented by sharp curvature regions.

Table 1 Crystal and refinement data for compounds **1–3**

	1	**2**	**3**
Empirical formula	$C_{38}H_{38}N_6O_{13}$	$C_{36}H_{30}N_4O_4$	$C_{28}H_{24}Br_4N_4O_4$
Formula weight	786.74	582.64	800.15
Crystal system	Triclinic	Monoclinic	Triclinic
Space group	$P\bar{1}$	$C2/c$	$P\bar{1}$
a, Å	7.8062(7)	17.2164(10)	8.8932(5)
b, Å	9.5179(6)	13.8834(5)	9.5548(6)
c, Å	12.7794(7)	15.0708(7)	10.0347(6)
α, °	104.468(2)	90	111.5900(10)
β, °	94.8020(10)	122.723(5)	91.2340(10)
γ, °	90.506(2)	90	115.4950(10)
V, Å^3	915.72(11)	3030.6(3)	699.01(7)
Z	1	4	1
D_{calc}, g/m^3	1.427	1.277	1.901
μ, mm^{-1}	0.109	0.085	5.800
$F(000)$	412	1224	392
Crystal size, mm	0.22×0.21×0.18	0.28×0.26×0.25	0.26×0.25×0.22
Total reflections	13,616	16,019	21,190
Unique reflections	4554	3099	3429
R_{int}	0.0253	0.0431	0.0490
GOF	1.020	1.054	1.038
R_1 $(I>2\sigma(I))$	0.0535	0.0426	0.0261
wR_2 $(I>2\sigma(I))$	0.1362	0.1039	0.0700
$\Delta\rho$max, eÅ^{-3}	0.21	0.26	0.49
$\Delta\rho$min, eÅ^{-3}	− 0.26	− 0.22	− 0.52

Table 2 Geometrical parameter for hydrogen bonds in compounds **1–3**

	D–H···A	D–H (Å)	H···A (Å)	D···A (Å)	D–H···A (Å)
1	N1–H1···O1	0.86	1.83	2.662(2)	161
	O1W–H1WA···O4^i	0.85	1.95	2.790(6)	170
	OW–H1WB···O1^{ii}	0.85	2.04	2.870(5)	167
	O3–H3···O2^i	0.86(2)	1.69(2)	2.544(2)	171.3(2)
	C4–H4···O3^i	0.93	2.40	3.175(2)	141
	C9–H9B···O1W^{iii}	0.96	2.32	3.241(6)	160
2	O1–H1···N1^i	0.82	1.84	2.634(3)	164
	C3–H3A···O2^{ii}	0.97	2.31	3.237(3)	159
	C3–H3B···O2^{iii}	0.97	2.41	3.318(2)	155
3	N2–H2···O2	0.86	1.74	2.582(2)	165
	C11–H11B···O1^i	0.97	2.44	3.172(3)	132

Symmetry codes for **1**: i=1-x, 1-y, 2-z, ii=x, − 1+y, z, iii=x, 1+y, z; for **2**: i=− 1+x, y, − 1+z, ii=1/2-x, 1/2-y, 1-z, iii=1/2+x, 1/2-y, 1/2+z; for **3**: i=1-x, 1-y, 1-z

Table 3 Geometrical parameter for π–π interactions in compounds **1**–**2**

	Rings I–J	Cg–Cg	α (°)	β (°)	γ (°)	CgI_Perp (Å)
1	Cg(1)–Cg(1)[iv]	3.624(1)	0	17.51	17.51	3.4564(7)
	Cg(1)–Cg(2)[iv]	3.633(1)	1.39(10)	16.55	17.87	3.4580(7)
	Cg(3)–Cg(3)[v]	3.798(1)	0	24.58	24.58	3.4537(7)
2	Cg(1)–Cg(1)[iv]	3.431(9)	0	9.17	9.17	3.3875(6)

Symmetry codes for **1**: iv = -x, 1-y, 1-z, v = 1-x, 2-y, 2-z; for **2**: iv = 3/2-x, 1/2-y, 2-z

For **1**: Cg(1): N1–C10–N2–C16–C11, Cg(2): C11–C12–C13–C14–C15–C16, Cg(3): C1–C2–C3–C4–C5–C6; For **2**: Cg(1): N1–C5–C9–N2–C11

Cg–Cg: distance between ring centroids, α: dihedral angle between planes I and J; β and γ: slipping angles; CgI_Perp: perpendicular distance of Cg(I) on ring J

The large flat areas with the blue outline indicate the π–π stacking interaction. A pair distance (de, di) for each Hirshfeld surface spot is used to generate the 2D fingerprint plots.

Results and discussion

Single-crystal X-ray diffraction experiment

Crystal structure of [(H$_2$L1)$^{2+}$·2(Hnip)$^-$·H$_2$O] (1)

Co-crystal **1** crystallizes as colorless cuboid-shaped crystals, representing the Triclinic $P\bar{1}$ space group. The repeating unit of **1** includes one half of L1 and one entire of H$_2$nip ligand and one half of water molecule (Fig. 1a). In the 5-nitroisophthalic acid groups, the lengths of C−O bond are C7−O3 = 1.306(2) Å, C7−O4 = 1.204(2) Å, C8−O1 = 1.243(2) Å, C8−O2 = 1.250(2) Å. The differences (Δ) between C7−O3 and C7−O4, C8−O1 and C8−O2 are 0.102 Å and 0.007 Å, respectively, which indicate the acid moiety C7 manifested as –COOH, nevertheless C8 manifested as −COO$^-$. The water molecules and H$_2$nip are involved in the construction of a 1D chain via O−H⋯O (O1W−H1WA⋯O4^i distance of 1.95 Å and the angle of 170°, O1W−H1WB⋯O1^{ii} distance of 2.04 Å the angle of 167°, O3−H3⋯O2^i distance of 1.69(2) Å and the angle of 171.3(2)°, Symmetry code: i = 1−x, 1−y, 2−z, ii = x, -1+y, z,) and C4−H4⋯O3^i (2.40 Å, 141°). The lengths of C−N bond are listed in Table S1. The lengths of C(10)−N(1) and C(11)−N(1) are shorter than the lengths of the deprotonated L1 [29], which is due to the fact that the N1 involved in producing N1−H1⋯O1 (1.83 Å, 161°) interactions. The bond lengths of C–O and C–N are in the normal range (Table 4). L1 ligands link neighboring 1D chain through the N1−H1⋯O1 interactions to form a 2D sheet in the *bc* plane (Fig. 1b). In addition, through the π–π interaction, the 2D network is further constituted to a 3D supramolecular framework along the *a*-axis direction, and the relevant parameters are listed in Table 3 (Fig. 1c).
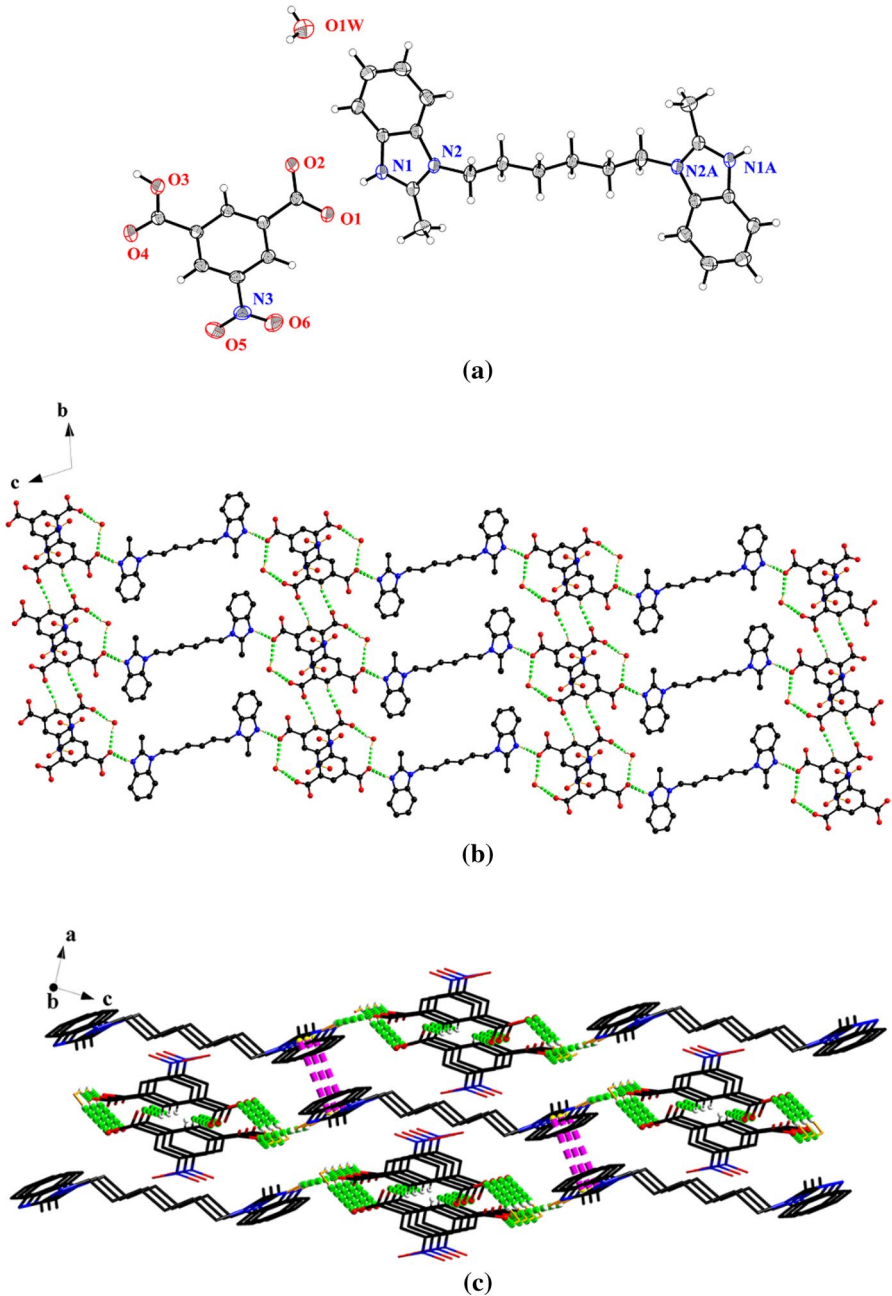
Fig. 1 **a** The ORTEP figure of co-crystal **1** with 30% thermal ellipsoids. **b** The 2D sheet structure formed through hydrogen bond interactions (green) in **1**. **c** The 3D supramolecular framework generated through hydrogen bond and $\pi-\pi$ interactions (pink) in **1**. (Color figure online)

Table 4 Comparison between C–O and C–N in the different samples

Co-crystal	C–O (Å)	C–N (Å)	References
1	1.204(2)–1.306(2)	1.327(2)–1.474(2)	This work
2	1.217(2)–1.321(2)	1.325(2)–1.461(2)	This work
3	1.226(2)–1.262(2)	1.331(3)–1.473(2)	This work
$[(H_2L1)^{2+}\cdot2(H_2btrc)^{1-}]$	1.217(2)–1.306(2)	1.326(3)–1.471(2)	[32]
$[(H_2L2)^{2+}\cdot(H_2btec)^{2-}\cdot2H_2O]$	1.218(3)–1.301(3)	1.329(3)–1.474(3)	[32]
$[(H_2L3)^{2+}\cdot(H_2btec)^{2-}]$	1.219(3)−1.298(3)	1.324(3)–1.472(3)	[32]

L1 = 1,3-bis(2-methylbenzimidazole)propane, L2 = 1,4-bis(2-methylbenzimidazole)butane, L3 = 1,4-bis(2-methylbenzimidazol-1-ylmethyl)benzene, H_3btrc = 1,2,4-benzenetricarboxylic acid, H_4btec = 1,2,4,5-benzenetetracarboxylic acid

Crystal structure of $[(L2)\cdot(H_2ndc)]$ (2)

Co-crystal **2** crystallizes in the monoclinic *C*2/*c* space group. The asymmetric unit of **2** contains a half of L2 and H_2ndc ligand (Fig. 2a). The Δ of C−O bonds are 1.217(2) Å (O2−C16) and 1.321(2) Å (O1−C16) of the H_2ndc ligand are for the COOH group. The difference in C−O bonds is 0.104 Å, which confirmed that the carboxyl groups of the H_2ndc are not deprotonated. The lengths of C−N are N1−C11 = 1.325 Å, N1−C5 = 1.392(2) Å, N2−C11 = 1.364(2) Å, N2−C9 = 1.384(2) Å. The (Δ) between N1−C11 and N1−C5 is 0.067 Å, between N2−C11 and N2−C9 is 0.02 Å, which is as a result of the formation of O1−H1···N1 (2.634(3) Å) hydrogen bond. The bond lengths of C–O and C–N are all in the normal range compared with the reported bond angles (Table 4). L2 ligands and H_2ndc ligands could install into a 1D *zigzag* chain, because of the presence of the O1−H1···N1 bonds between the nitrogen atoms of the L2 ligands and the carboxyl groups of the H_2ndc ligands (Fig. S1). In addition, there is a π–π interaction between two different imidazole rings of two distinct L2 ligands with the distance of Cg1−Cg1^{iv} is 3.431(9) Å (Cg(1): N1−C5−C9−N2−C11, Symmetry code: iv = 3/2-*x*, 1/2-*y*, 2-*z*). The 1D chains are linked by the π–π interaction to form a 2D network in the axes a and c (Fig. 2b). C–H···O hydrogen bonds stabilize this 2D structure.

Crystal structure of $[(H_2L3)^{2+}\cdot(tbta)^{2-}]$ (3)

3 belongs to the Triclinic *P*1̄ space group. The repeating unit of **3** composed by a half of L3 and H_2tbta ligand (Fig. 3a). In the carboxylic, the bond distances of O1−C12 and O2−C12 are 1.226(2) Å and 1.262(2) Å, respectively, the Δ of O−C is 0.036 Å, which means the H_2tbta acid molecule is completely deprotonated. Meanwhile, the plane of the two benzimidazole rings on the same L3 is parallel, and the L3 ligand takes *anti*-conformation. The Δ values of N1−C9 and N1−C2, N2−C2 and N2−C4 are 0.044 Å and 0.045 Å, which are very close. The bond lengths of C–O and C–N are comparable to those found in other co-crystals (Table 4). There are N−H···O intermolecular interactions between the O2 atoms of tbta^{2-} ligands and N2 atoms
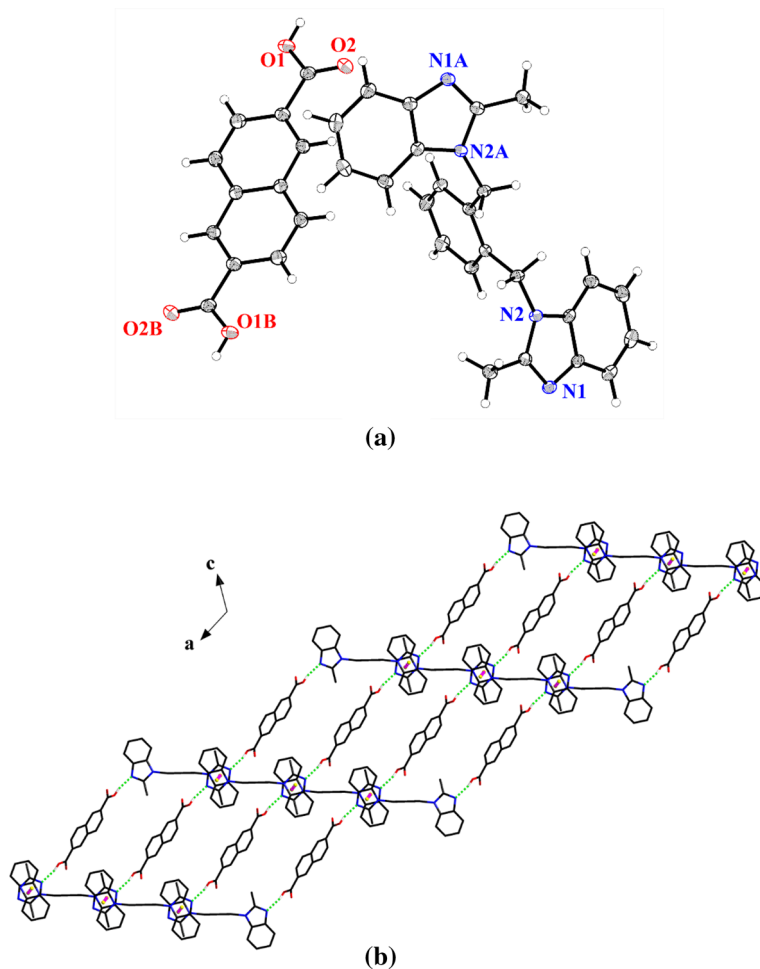
(a)

(b)

Fig. 2 **a** The ORTEP figure of co-crystal **2** with 30% thermal ellipsoids. **b** The 2D network structure generated through hydrogen bond (green) and $\pi-\pi$ interactions (pink) in **2**. (Color figure online)

of L3 ligands (N2−H2···O2 (2.583(3) Å). L3 and tbta^{2-} ligands build up a1D *zigzag* chain through the N2−H2···O2 intermolecular interactions. Furthermore, there are C−H···O interactions between the L3 and tbta^{2-} ligands, the *zigzag* chain is further extended into a 2D sheet network by the hydrogen bonds alone the axes a and b (Fig. 3b).

IR spectra

As shown in Fig. S2, IR spectra of **1**, **2** and **3** show some weak bonds around 3000 cm^{-1} (3092 cm^{-1} for **1**, 3000 cm^{-1} for **2** and 3100 cm^{-1} for **3**), which are a result of the $\nu_{(C-H)}$ stretching vibration of the benzimidazole rings. The significant

(a)

(b)

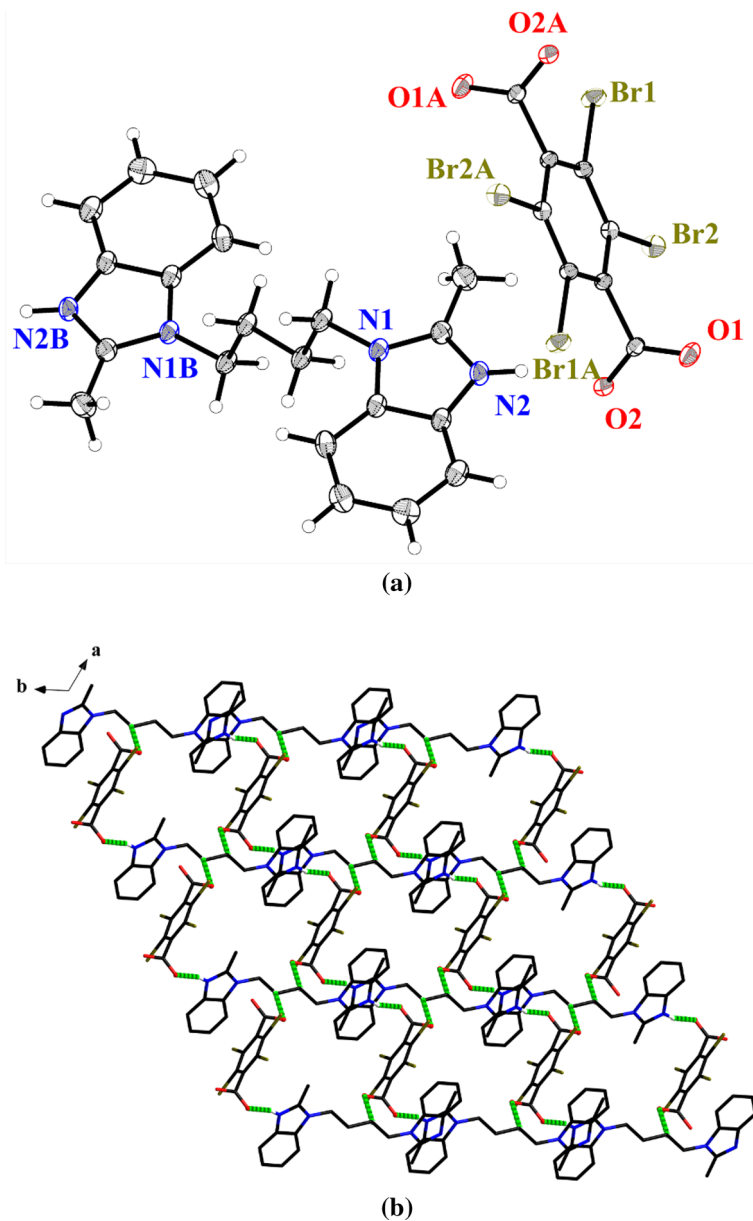**Fig. 3 a** The ORTEP figure of **3** with 30% thermal ellipsoids. **b** The 2D network structure generated through hydrogen bond interactions (green) in **3**. (Color figure online)

characteristic peak of **1** round 3400 cm^{-1} attributes to the O−H stretching vibration modes of water molecules. There are obvious bonds near 1700 cm^{-1}, which are assigned to the carboxylate groups of **1** and **2**. The asymmetric and symmetric

Table 5 Comparison of the vibrations in the 1, 2 and 3 with similar structures

Co-crystal	Asymmetric (cm^{-1})	Symmetric (cm^{-1})	References
1	1630	1376	This work
2	1600	1424	This work
3	1640	1423	This work
$[(H_2L1)^{2+}\cdot(tca^-)_2]$	1616	1380	[33]
$[(H_2L2)^{2+}\cdot(3\text{-Hnpa}^-)_2\cdot 3H_2O]$	1610	1404	[33]
$[(H_2L3)^+_{0.5}\cdot(4\text{-Hnpa}^-)\cdot H_2O]$	1622	1394	[33]
$[(HL4)\cdot(3,5\text{-dns}^-)]$	1610	1392	[33]
$[(H_2L4)^{2+}\cdot(3\text{-npa}^{2-})]$	1612	1394	[33]
$[(H_2L3)\cdot(pam)]$	1626	1418	[33]

L1 = 3,6-bis(imidazole-1-yl)pyridazine, Htca = trichloroacetic acid, L2 = bis(*N*-imidazolyl)meth-ane, 3-H$_2$npa = 3-nitrophthalic acid, L3 = bis(N-imidazolyl)butane, 4-H$_2$npa = 4-nitrophthalic acid, L4 = 1-(3-(1H-benzimidazol-1-yl)propyl)-1H-benzimidazole, 3,5-Hdns = 3,5-dinitrosalicylic acid, pam = pamoic acid
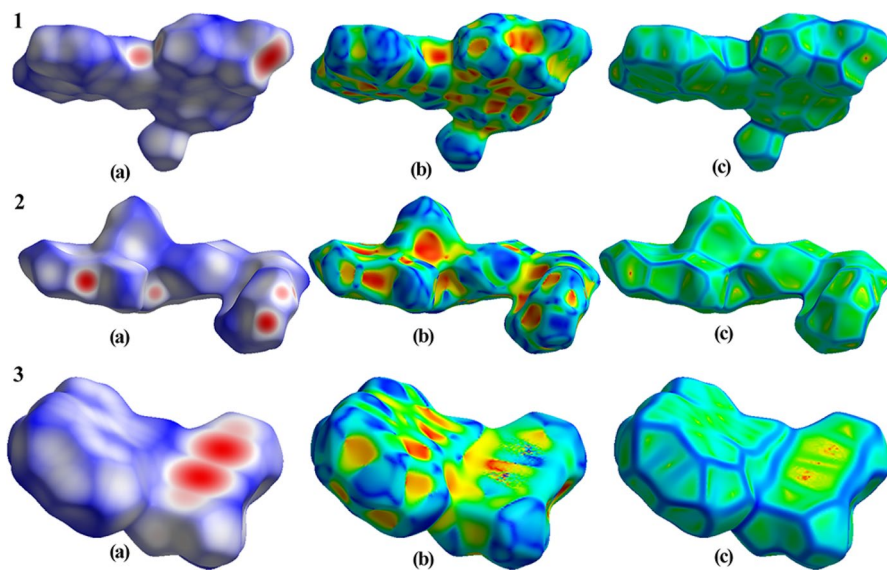
Fig. 4 The Hirshfeld surface with d_{norm} (**a**), *Shape index* (**b**) and *Curvedness* (**c**) for **1**, **2**, **3**

stretching vibrations of the carboxylate groups in **1**, **2** and **3** are observed in the range of 1370–1640 cm^{-1}. The asymmetric and symmetric vibrations of carboxylate group in the **1**, **2** and **3** are compared with those in literature for similar structures (Table 5). The $\nu_{(C=N)}$ stretching vibration of the N-containing ligands correspond to absorbance bands of 1531 cm^{-1} for **1**, 1508 cm^{-1} for **2** and 1465 cm^{-1} for **3**.

Hirshfeld surface

As shown in Fig. 4, the 3D Hirshfeld surfaces of **1**−**3** illustrate that each given crystal structure possesses distinct Hirshfeld surfaces, which evidently demonstrates that different building blocks play a key role on the intermolecular contacts. The close-contact interaction can be expressed as deep and large red spots on the d_{norm} surfaces, which primarily refers to the important hydrogen bond interactions, for instance, the interactions of N−H···O and O−H···O. In addition, on the d_{norm} surfaces, the C–H···O contacts are displayed as small red circular spots, and the H···H interactions are exhibited as other visible spots. The *Curvedness* of **1**–**3** indicates that in **1** and **2**, π–π interactions play an important role in the formation of the structure, while in **3**, π–π interactions have little effect on the structure.

The 2D fingerprint plots and percentage contributions of various intermolecular interactions for **1**–**3** are also investigated. Based on the support of Fig. 5, distinct contacts that usually overlap each other in the full fingerprint plots can be disconnected, 2D fingerprint plots of **1**–**3** evidence different appearances, which are caused by distinct structures and diverse intermolecular interactions. For **1**, in the middle of distributed points in the 2D fingerprint plots, the second most important to the entire Hirshfeld surfaces (34.3%) represent the H···H contacts, and the two double peaks represent the H···O interaction, which is the most important intermolecular interactions for the entire Hirshfeld surface (36.1%) (Fig. 6). In **2** and **3**, for the entire Hirshfeld surface, the most important is the H···H contacts (41.7% of **2**, 22.0% of **3**) in the middle of the figure. For **2** and **3**, the contacts of H··O and O···H appear as two single peaks, which account for 15.0% and 21.7% of the Hirshfeld surface of each molecule, while the proportion of H···C and C···H interactions comprises 16.0% for **1**, 31.8% for **2** and 14.5% for **3**, respectively, which reflected as points at the wings of the 2D fingerprint plots.

Thermal properties

The TG curves show that **1** own three weight loss steps, while both **2** and **3** own two dissimilar weight loss steps (Fig. 7). For **1**, the first stage is the decomposition of lattice water molecules (found. 2.6%, calcd. 2.3%) from 97 °C to 151 °C. Then, with the increase in temperature, the following mass loss steps can be regarded as the breakdown of L1 in the range of 285–405 °C (found. 43.9% calcd 44.0%). From 435 °C to 634 °C, the loss of weight corresponds to the H_2nip (found. 53.5%, calcd. 53.7%). For **2**, the L2 weight loss occurs from 253 °C to 295 °C (found. 62.7%, calcd. 62.9%), the second weight loss from 295 °C to 600 °C is ascribed to H_2ndc (found. 37.3%, calcd. 37.1%). For **3**, the weight loss from 222 °C to 265 °C can be assigned to H_2tbta (found. 60.4%, calcd. 60.2%). The weight loss happening from 265 °C to 454 °C is because of the release of L3 (found. 39.6, calcd. 39.8).

Photoluminescent properties

In the solid state, the photoluminescent spectra of **1**–**3** and their corresponding molecular components were inspected. As shown in Fig. 8, the photoluminescent
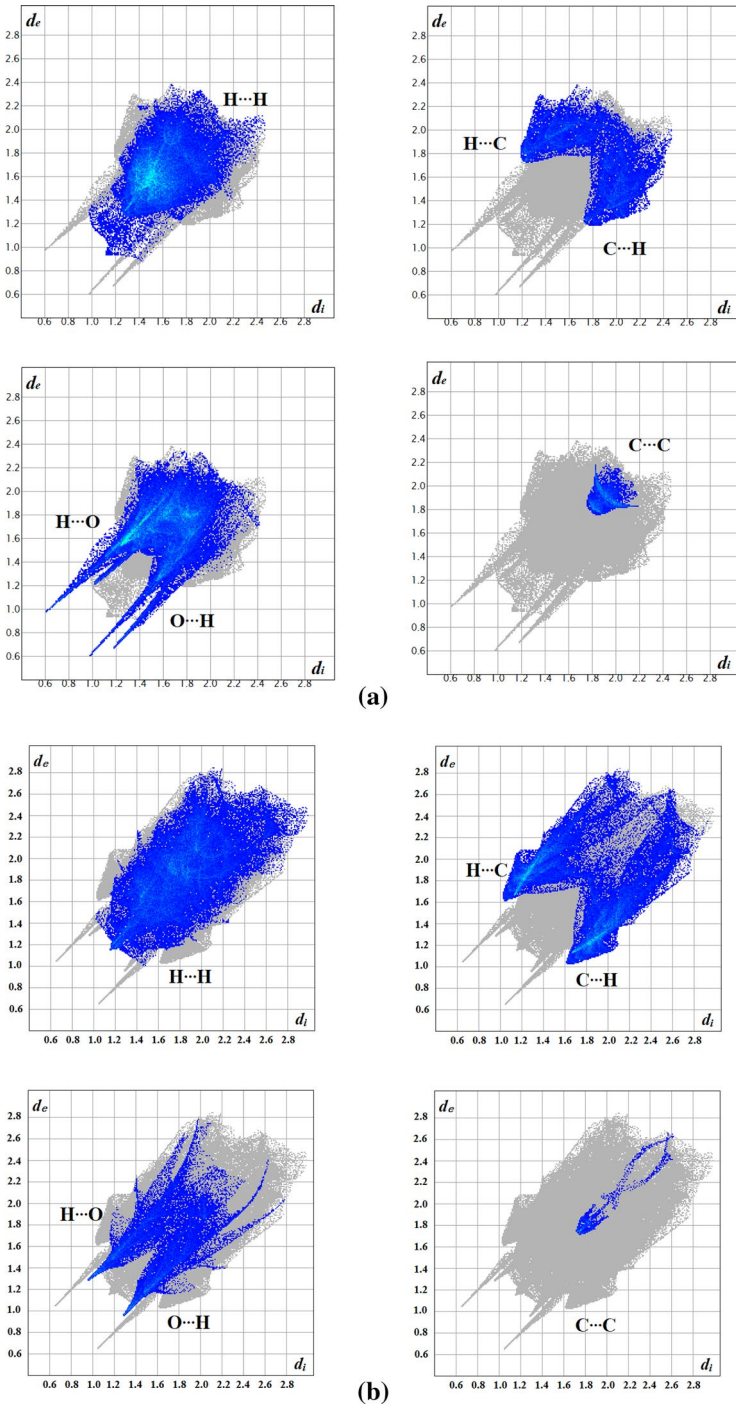
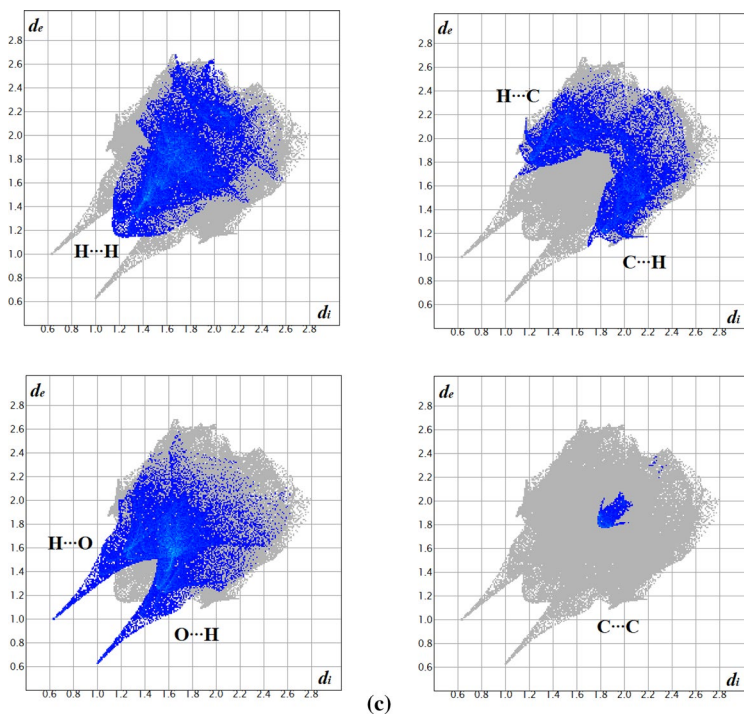**Fig. 5** The 2D fingerprint plots for **1** (**a**), **2** (**b**), **3** (**c**)
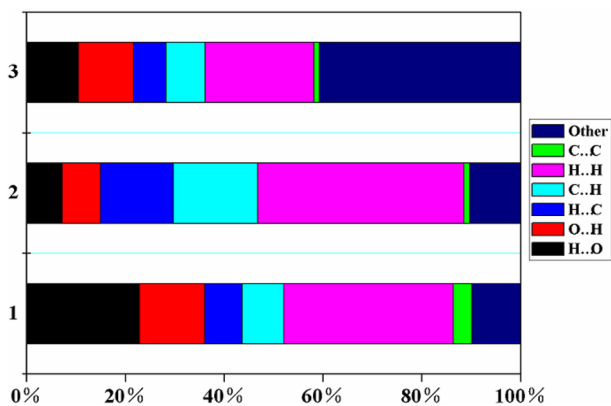
(c)

Fig. 5 (continued)

Fig. 6 The relative percentage contributions to the Hirshfeld surface area for various intermolecular contacts in compounds **1–3**

spectra of free L1, L2, L3, H_2nip, H_2ndc and H_2tbta display the maximum emissions at 305, 302, and 308, 480, 402, and 338 nm, which excitation at 282, 282, 240, 241, 279 and 283 nm, individually. The phenomena are ascribed to the $n \rightarrow \pi^*$ or $\pi \rightarrow \pi^*$ transition. Furthermore, compounds **1–3** adopt
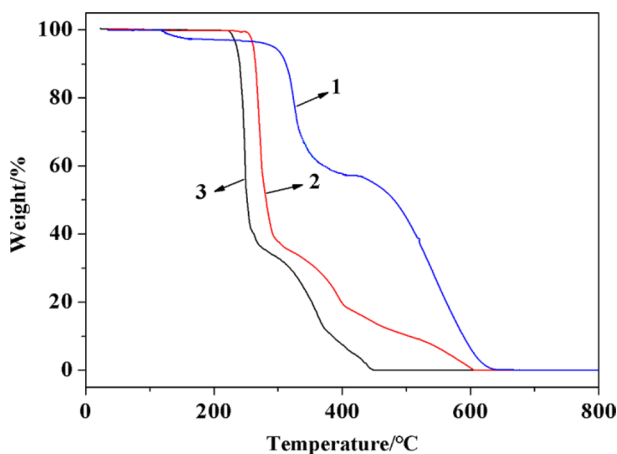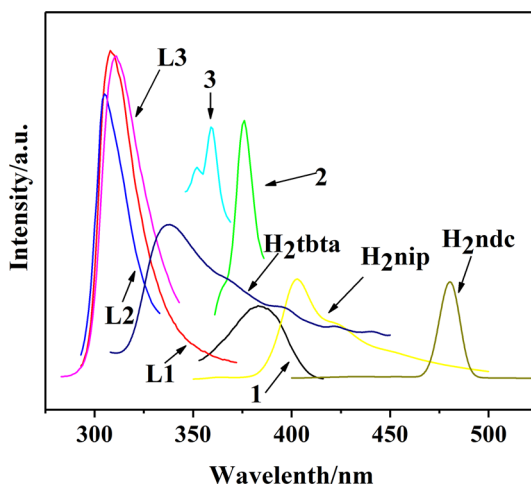
Fig. 7 The TG curves of compounds **1**–**3** under N_2 atmosphere

Fig. 8 The photoluminescent spectra of compounds **1**–**3** and the free ligands

similar photoluminescent emissions bonds at 380 nm ($\lambda_{ex} = 314$ nm), 373 nm ($\lambda_{ex} = 297$ nm) and 356 nm ($\lambda_{ex} = 295$ nm), respectively. Compared with L1, L2 and L3 ligands; the photoluminescent spectra of **1**, **2** and **3** exhibit redshifted 75 nm, 71 nm and 48 nm, individually, which may be attributed to the hydrogen bonds in **1**, **2** and **3** [30, 31]. In addition, the photoluminescent spectra of **1** and **2** disclose blueshifted 100 nm and 29 nm relative to the H_2nip, H_2ndc. For **3**, the photoluminescent spectrum displays redshifted 18 nm. These phenomena may be caused by $\pi \rightarrow \pi^*$ intraligand transitions because they are very similar to the emission bands of the corresponding carboxylic acid ligands [32].

Conclusion

In this work, three co-crystals **1, 2** and **3** based on aromatic carboxylic acids and bis(benzimidazole) derivatives were synthesized and characterized. In particular, the single-crystal X-ray diffraction and Hirshfeld surface provide detailed analysis into the intermolecular interaction and the types of contacts supplying noteworthy effect on the compounds **1–3**. For **1**, the 2D sheet was generated through O–H···O, C–H···O and N–H···O interactions, which is further expanded into a 3D supramolecular framework via π–π interactions. For **2**, the 2D structure was constructed by O–H···N hydrogen bonds and π–π interactions. In **2**, the C–H···O hydrogen bonds serve to make structures more stable. For **3**, the 2D network was generated by two different types of hydrogen bonds (N–H···O and C–H···O). Additionally, in the solid state, all compounds hold fascinating luminescence properties.

Supplementary data

CCDC 1,862,567, 1,482,024 and 1,862,566 contain the supplementary crystallographic data for compounds **1–3**. These data can be attained free of charge via https://www.ccdc.cam.ac.uk/conts/retrieving.html, or from the Cambridge Crystallographic Data Centre, 12 Union Road, Cambridge CB2 1EZ, UK; fax: (+44) 1223–336-033; or e-mail: deposit@ccdc.cam.ac.uk.

Compliance with Ethical Standards

Conflict of interest The authors declare that they have no conflict of interest.

References

1. P. Vishweshwar, J.A. McMahon, M.L. Peterson, M.B. Hickey, T.R. Shattock, M.J. Zaworotko, Chem. Commun. **36**, 4601 (2005)
2. B. Gao, D.J. Wang, J. Zhang, Y.J. Hu, J.P. Shen, J. Wang, B. Huang, Z.Q. Qiao, H. Huang, F.D. Nie, G.C. Yang, Mater. Chem. A **2**, 19969 (2014)
3. C.B. Aakeröy, I. Hussain, S. Forbes, J. Desper, CrystEngComm **9**, 46 (2007)
4. G.G. Hou, H.J. Zhao, J.F. Sun, D. Lin, X.P. Dai, J.T. Han, H. Zhao, CrystEngComm **15**, 577 (2013)
5. M.I. Hashim, H.T.M. Le, T.H. Chen, Y.S. Chen, O. Daugulis, C.W. Hsu, A.J. Jacobson, W. Kaveevivitchai, X. Liang, T. Makarenko, O.S. Miljanic, I. Popovs, H.V. Tran, X. Wang, C.H. Wu, J.I. Wu, Am. Chem. Soc. **140**, 6014 (2018)
6. C.B. Aakeröy, K.R. Seddon, Chem. Soc. Rev. **22**, 397 (1993)
7. S.D. Feyter, F.C. De Schryver, Chem. Soc. Rev. **32**, 139 (2003)
8. S.W. Jin, D.Q. Wang, J. Chem. Crystallogr. **40**, 914 (2010)
9. E. Kolomiets, E. Buhler, S.J. Candau, J.M. Lehn, Macromolecules **39**, 1173 (2006)
10. D.C. Sherrington, K.A. Taskinen, Chem. Soc. Rev. **30**, 83 (2001)
11. D.P. Yan, A. Delori, G.O. Lloyd, B. Patel, T. Friščić, G.M. Day, CrystEngComm **14**, 5121 (2012)

12. L.H. Zhai, L.H. Guo, Y. Ling, H.S. Wu, J.W. Wang, B.W. Sun, Y.H. Luo, Res. Chem. Intermed. **43**, 817 (2016)
13. S.L. Tan, E.R.T. Tiekink, Z. Kristallogr, NCS. **234**, 1109 (2019)
14. M. Lou, S.H. Mao, Y.H. Luo, P. Zhao, B.W. Sun, Res. Chem. Intermed. **41**, 2939 (2013)
15. G.C. Liu, J.J. Huang, J.W. Zhang, X.L. Wang, H.Y. Lin, Transit. Met. Chem. **38**, 359 (2013)
16. E.R. Adriana, G.G. Guadalupe, M. Edgar, P.H. Adrian, L.S. Horacio, F.P. Angelina, C. Rosalinda, B.B. Norah, Dalton Trans. **39**, 6302 (2010)
17. C.H. Jiao, J.C. Geng, C.H. He, G.H. Cui, J. Mol. Struct. **1020**, 134 (2012)
18. S. Samai, K. Biradha, Cryst. Growth Des. **11**, 5723 (2011)
19. X.X. Wang, Y.J. Ma, H.H. Li, G.H. Cui, Transit. Met. Chem. **40**, 99 (2014)
20. X.L. Wang, Z.Q. Xia, W. Wei, G. Xie, S.P. Chen, S.L. Gao, J. Chem. Thermodyn. **55**, 124 (2012)
21. Y. Gong, Y.C. Zhou, T.F. Liu, J. Lu, D.M. Proserpio, R. Cao, Chem. Commun. **47**(21), 5982 (2011)
22. L. Wang, Z.H. Yan, Z.Y. Xiao, D. Guo, W.Q. Wang, Y. Yang, CrystEngComm **15**, 5552 (2013)
23. S.K. Seth, D. Sarkar, T. Kar, CrystEngComm **13**, 4528 (2011)
24. H.F. Clausen, M.S. Chevallier, M.A. Spackman, B.B. Iversen, New J. Chem. **34**, 193 (2010)
25. M.A. Spackman, D. Jayatilaka, CrystEngComm **11**, 19 (2009)
26. G.M. Sheldrick, Acta Crystallogr. Sect. A **64**, 112 (2008)
27. T. Gelbrich, M.B. Hursthouse, CrystEngComm **7**, 324 (2005)
28. F.L. Hirshfeld, Theor. Chim. Acta. **44**, 129 (1977)
29. H. Zhu, D. Liu, Y.H. Li, G.H. Cui, Polyhedron **167**, 44 (2019)
30. Z.J. Zhang, W. Shi, Z. Niu, H.H. Li, B. Zhao, P. Cheng, D.Z. Liao, S.P. Yan, Chem. Commun. **47**, 6425 (2011)
31. Y.H. Ma, M. Lou, Q.Y. Sun, S.W. Ge, B.W. Sun, J. Mol. Struct. **1083**, 111 (2015)
32. J.W. Cui, Y.Q. Zhao, Z.C. Hao, G.H. Cui, Res. Chem. Intermed. **44**, 721 (2017)
33. A. Ding, S. Jin, S. Jin, K. Hu, Z. Lin, H. Liu, D. Wang, J. Mol. Struct. **1151**, 17 (2018)